FINITE-ELEMENT MODELING OF DEFORMATION AND CRACKING IN EARLY-AGE CONCRETE

By René de Borst[1] and A. H. van den Boogaard[2]

ABSTRACT: The main nonlinear phenomena that govern the deformational behavior of early-age concrete are the evolution of the stiffness properties, the development of thermal strains, creep, and cracking. A general approach for numerically simulating this type of behavior is presented. The thermomechanical problem is decoupled such that first a thermal analysis is carried out and then a stress calculation is performed. An interface program is used to map the results from the thermal analysis onto the input data required for the stress analysis. A brief review of the relations for the thermal-stress analysis is given, followed by a more elaborate treatment of the algorithm used for the combination of thermal strains, creep, and smeared cracking. To properly accommodate these effects in a finite-element analysis, a smeared-crack model is used that is rooted in a decomposition of the strain increments. The emphasis is on the general approach for properly and efficiently handling these phenomena. A special case, namely a power-type creep law, is elaborated. It is shown that this relationship reasonably fits experimental data. A detailed description of an example calculation that demonstrates the potential of the numerical simulation strategy follows.

INTRODUCTION

The chemical processes that occur during hardening of young concrete in the first few days after casting are accompanied by significant volume and temperature changes. Initially, heat is generated, and while the stiffness of the concrete mass is low, the overall volumetric expansion of the concrete results in moderate (mainly compressive) stresses. In the second phase, the concrete mass starts to cool down and, because the stiffness has markedly increased, significant tensile stresses develop. The ensuing cracks are present before the structure has ever been loaded.

The damage induced at this moment has major consequences for the long-term structural performance of the concrete structure, and on its durability and serviceability. Early-age cracking favors corrosion of the reinforcement, carbonation, and long-term chemical phenomena such as alkali-silica reaction. It is disastrous when environmentally protective reinforced concrete structures are concerned, such as buildings for storage of chemical and radioactive waste, nuclear containment vessels, liquefied natural gas tanks, and storage tanks for chemicals, as well as common structures such as leakage-tight floors of gas stations and tanks for liquid manure in the agricultural industry.

A better understanding of the mechanisms that play a role during hydration of early-age concrete as well as a proper assessment of the technological measures that can be taken to prevent cracking in early-age concrete (use of additives, cooling pipes, staged construction procedures), can

[1]Prof. of Civ. and Mech. Engrg., Delft Univ. of Technol. and Eindhoven Univ. of Technol., P.O. Box 5048, 2600 GA Delft, The Netherlands.

[2]Res. Engr., TNO Build. and Constr. Res., P.O. Box 49, 2600 AA Delft, The Netherlands.

Note. Discussion open until May 1, 1995. To extend the closing date one month, a written request must be filed with the ASCE Manager of Journals. The manuscript for this paper was submitted for review and possible publication on June 18, 1993. This paper is part of the ***Journal of Engineering Mechanics***, Vol. 120, No. 12, December, 1994. ©ASCE, ISSN 0733-9399/94/0012-2519/$2.00 + $.25 per page. Paper No. 6400.

only be obtained if combined experimental and numerical investigations are undertaken. While there is a reasonable amount of experimental data available in the literature, publications on numerical procedures for analyzing the deformational behavior, including crack initiation and propagation in young concrete, are virtually absent. An exception is an early paper by van den Bogert et al. (1987), which, however, does not consider cracking.

In the present paper, we focus on the further development of numerical strategies for the deformational and fracture behavior of early-age concrete. To this end we first outline the general strategy one can follow in numerical approaches to this problem. Then, we briefly touch on issues like heat generation and evolution of the elastic stiffness in a solidifying system like young concrete. We do not present new models for the individual nonlinear phenomena. The major contribution is the consistent formulation for the combined action of these nonlinearities and their interaction with fracture. With this formulation, a stable and robust algorithm for creep and combined creep-fracture analyses is developed. The present paper concludes with an example of stress and crack development in a cover element of a breakwater (a tetrapod).

FINITE-ELEMENT PROCEDURES FOR THERMAL AND STRESS ANALYSIS IN EARLY-AGE CONCRETE

Stress evolution and cracking in early-age concrete is basically a coupled thermomechanical problem. Because in the present case the coupling is rather weak, the thermal and mechanical problems are decoupled. A two-stage procedure follows, in which the thermal problem is solved first. The temperatures and other state variables (e.g., the degree of maturity, see the following) that result from the thermal analysis serve as input for the computation of the stress evolution including the initiation and propagation of cracking.

An interface program is used to map the temperatures and other state variables that are computed in the discretization used for the thermal analysis onto the discretization that is used for the stress analysis. Two effects have to be taken into account in such an interface program. First, different discretizations and different types of elements are normally used for both analyses, which is motivated by the need to use an element for the stress analysis with an interpolation polynomial that is an order higher than the interpolation polynomial used in the heat-conduction problem. Only then, spatially oscillating stress fields are avoided. Secondly, the temperatures are primary variables in the heat-conduction analysis, and are hence computed in the nodes, but needed in the integration points of the new discretization to be used in the stress analysis. Because of both reasons, an interpolation procedure must be carried out to obtain the temperatures in the integration points of the discretization that is used in the stress analysis. Interpolations must also be carried out to transfer the state variables that are computed during the thermal analysis in the "old" integration points to the integration stations used in the stress analysis.

HEAT PRODUCTION AND STIFFNESS EVOLUTION

The hydration process in early-age concrete can be characterized by different parameters (e.g., Reinhardt et al. 1982; van Breugel 1991). Here we shall follow Reinhardt et al., who used the so-called degree of maturity $r(t)$,

which is defined as the quotient of the accumulated heat production at time t and the total heat production at infinity Q_∞

$$r(t) = \frac{1}{Q_\infty} \int_0^t q(\tau)\, d\tau \tag{1}$$

with the heat production q calculated using an Arrhenius type relation

$$q = \gamma f(r) \exp(-b/T) \tag{2}$$

where γ and b = material constants; T = absolute temperature (K); and $f(r)$ = heat-production function, which is determined experimentally and depends on, among other factors, the cement type. The function $f(r)$ that was used in the example calculations at the end of this contribution is shown in Fig. 1.

As stipulated in the introduction, the chemical processes that occur in the hardening cement paste strongly affect its mechanical properties, for example, the Young's modulus $E(t)$ and the coefficient of thermal expansion, as well as its thermal properties like the thermal conductivity λ and the heat capacity c. Following Reinhardt et al. (1982), see also de Borst (1989), we make E, λ, and c dependent on the state variable r. In the example calculations reported, the following simple relationships are adopted for λ and c:

$$\lambda = \lambda_0 - \lambda_1 r \tag{3}$$

and

$$c = c_0 - c_1 r \tag{4}$$

with λ_0, λ_1, c_0, and c_1 parameters. The following evolution formula for Young's modulus was used (Reinhardt et al. 1982):

$$E(t) = E_0 \int_0^t (T/T_0)^7 \{1 - \exp[(-\beta(t - \tau))/(T/T_0)^6]\} \dot{r}\, d\tau \tag{5}$$

In (5), E_0 = an elastic stiffness parameter, which depends on the amount and type of cement; β = a delay factor; and T_0 = 273 K.

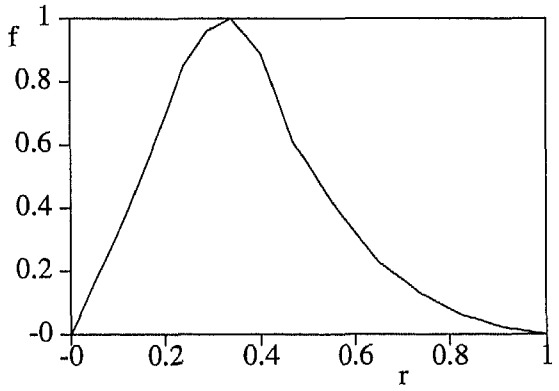

FIG. 1. Heat-Production Function $f(r)$ Used in Example Calculations

CONCRETE CREEP AND LARGE-SCALE COMPUTATIONS

As point of departure for the creep formulation we take (cf. Bažant et al. 1988)

$$\boldsymbol{\varepsilon}(t) = \int_0^t J(t, \tau)\mathbf{C}\dot{\boldsymbol{\sigma}}(\tau)\, d\tau \tag{6}$$

In (6), $\dot{\boldsymbol{\sigma}}$ = stress rate tensor; $J(t, \tau)$ = creep function; and the components of $\mathbf{C}$ are defined by

$$C_{ijkl} = \frac{1}{2}(1 + \nu)(\delta_{ik}\delta_{jl} + \delta_{il}\delta_{jk}) - \nu\delta_{ij}\delta_{kl} \tag{7}$$

where ν = Poisson's ratio, which is assumed to be independent of the time of load application $\tau = t$; and δ_{ij} = Kronecker delta.

We now consider the time interval $\Delta t = t_{i+1} - t_i$ and define the corresponding increments of stress and strain

$$\Delta\boldsymbol{\sigma} = \boldsymbol{\sigma}(t_{i+1}) - \boldsymbol{\sigma}(t_i) \tag{8}$$

and

$$\Delta\boldsymbol{\varepsilon} = \boldsymbol{\varepsilon}(t_{i+1}) - \boldsymbol{\varepsilon}(t_i) \tag{9}$$

Using (6) the strain increment is readily expressed

$$\Delta\boldsymbol{\varepsilon} = \int_0^{t_i} [J(t_{i+1}, \tau) - J(t_i, \tau)]\mathbf{C}\dot{\boldsymbol{\sigma}}(\tau)\, d\tau + \int_{t_i}^{t_{i+1}} J(t_{i+1}, \tau)\mathbf{C}\dot{\boldsymbol{\sigma}}(\tau)\, d\tau \tag{10}$$

The use of constitutive relations in displacement-method–based finite elements is greatly facilitated if the stress increment is explicitly written as a function of the strain increment and the strain or stress history. For this reason (10) is rearranged such that the stress increment $\Delta\boldsymbol{\sigma}$ is a function of the strain increment and the strain history. Assuming that the stress varies linearly over the time increment Δt: $\dot{\boldsymbol{\sigma}} \approx \Delta\boldsymbol{\sigma}/\Delta t$, using a generalized midpoint rule ($t_i \le t^* \le t_{i+1}$)

$$\bar{E}^{-1}(t^*) = \Delta t^{-1} \int_{t_i}^{t_{i+1}} J(t_{i+1}, \tau)\, d\tau \tag{11}$$

and introducing the dimensionless matrix $\mathbf{D} = \mathbf{C}^{-1}$, we obtain

$$\Delta\boldsymbol{\sigma} = \bar{E}(t^*)\left\{\mathbf{D}\Delta\boldsymbol{\varepsilon} - \int_{\tau=0}^{t_i} [J(t_{i+1}, \tau) - J(t_i, \tau)]\dot{\boldsymbol{\sigma}}(\tau)\, d\tau\right\} \tag{12}$$

Setting

$$\bar{\boldsymbol{\sigma}}(t_i) = -\bar{E}(t^*) \int_{\tau=0}^{t_i} [J(t_{i+1}, \tau) - J(t_i, \tau)]\dot{\boldsymbol{\sigma}}(\tau)\, d\tau \tag{13}$$

we obtain the following general expression for computing the stress increment in linear-viscoelastic, aging materials

$$\Delta\boldsymbol{\sigma} = \bar{E}(t^*)\mathbf{D}\Delta\boldsymbol{\varepsilon} + \bar{\boldsymbol{\sigma}}(t_i) \tag{14}$$

To circumvent storage of the entire load history of each material point as is implied by the supplied algorithm, the kernel $J(t, \tau)$ of the hereditary

integral is commonly expanded into a series of negative exponential powers (Dirichlet series) or polynomials (Taylor series). The first approach is usually adopted for long-term creep simulations, the period of consideration stretching over years to several decades (Zienkiewicz et al. 1968; Taylor et al. 1970; Bažant and Wu 1973, 1974). The other procedure can be advantageously used for short-term creep processes, for example, in early-age concrete (van den Bogert et al. 1987; de Borst et al. 1993; Anderson et al. 1988).

Dirichlet Series

Although the main theme of this contribution is concrete creep at early ages, we briefly discuss how a Kelvin chain, which is normally used for long-term concrete-creep simulations, can be derived from (12) to show the similarities with the numerical approach for concrete creep at early ages that is outlined next. For this purpose, we expand the creep function in a series of negative exponential powers (Dirichlet series)

$$J(t, \tau) = E_0^{-1}(\tau) + \sum_{\alpha=1}^{N} E_\alpha^{-1}(\tau)[1 - \exp(-(t - \tau)/\lambda_\alpha)] \tag{15}$$

Mechanically, the model can be interpreted as a Kelvin chain (Bažant and Wu 1973), with λ_α the retardation times of the individual elements of the chain. In consideration of (11), the instantaneous stiffness can then be elaborated as

$$\bar{E}^{-1}(t^*) = E_0^{-1}(t^*) + \sum_{\alpha=1}^{N} E_\alpha^{-1}(t^*)\{1 - [1 - \exp(-\Delta t/\lambda_\alpha)]\lambda_\alpha/\Delta t\} \tag{16}$$

The relaxation term $\tilde{\boldsymbol{\sigma}}(t_i)$ can be worked out as

$$\tilde{\boldsymbol{\sigma}}(t_i) = -\bar{E}(t^*) \sum_{\alpha=1}^{N} [1 - \exp(-\Delta t/\lambda_\alpha)]\tilde{\boldsymbol{\varepsilon}}_\alpha(t_i) \tag{17}$$

where the internal variables $\tilde{\boldsymbol{\varepsilon}}_\alpha$ are updated according to the recurrence formula (Zienkiewicz et al. 1968; Taylor et al. 1970; Bažant and Wu 1973)

$$\tilde{\boldsymbol{\varepsilon}}_\alpha(t_{i+1}) = \exp(-\Delta t/\lambda_\alpha)\tilde{\boldsymbol{\varepsilon}}_\alpha(t_i) + E_\alpha^{-1}(t^*)[1 - \exp(-\Delta t/\lambda_\alpha)](\lambda_\alpha/\Delta t)\mathbf{C}\Delta\boldsymbol{\sigma} \tag{18}$$

The accuracy of this integration scheme hinges on the assumption that $\dot{\boldsymbol{\sigma}}$ and E_α do not vary much during the time step. Indeed, this semianalytical integration procedure is exact if $\dot{\boldsymbol{\sigma}}$ and E_α are constant during the time step. For a nonaging or nonsolidifying solid, the assumption that E_α remains constant during a time step is satisfied rigorously. In the absence of cracks, the assumption that $\dot{\boldsymbol{\sigma}}$ remains constant is usually reasonable. When we have crack initiation or propagation, the assumption is more questionable. As we show hereafter, $\dot{\boldsymbol{\varepsilon}}$ must then be replaced by $\dot{\boldsymbol{\varepsilon}}^{co}$, the part of the total strain rate that applies to the concrete. Since $\dot{\boldsymbol{\varepsilon}}^{cr}$ can vary quite abruptly over a time step, $\dot{\boldsymbol{\varepsilon}}^{co}$ may also show considerable changes as does $\dot{\boldsymbol{\sigma}}$. This implies that time steps must be chosen much smaller when cracks appear.

Taylor Series

For creep in early-age concrete only relatively short time spans have to be analyzed. On the other hand, the stress fluctuations during this period may be more pronounced than in "long-term" processes. For this reason, it may be advantageous to develop $J(t, \tau)$ in a Taylor series instead of in a Dirichlet series. We consider the class of creep functions for which

$$J(t, \tau) = E^{-1}(\tau) + f(\tau) \cdot g(t - \tau) \tag{19}$$

which is sufficiently broad to encompass most commonly used creep models. Expanding $g(t - \tau)$ in a Taylor series around $\tau = t_d$ gives

$$g(t - \tau) = \sum_{\alpha=0}^{N} h_\alpha (t - t_d)\tau^\alpha \tag{20}$$

where, for instance, for $N = 5$

$$h_0 = a_0 + a_1(t - t_d) + a_2(t - t_d)^2 + a_3(t - t_d)^3 + a_4(t - t_d)^4 + a_5(t - t_d)^5 \tag{21}$$

$$h_1 = -a_1 - 2a_2(t - t_d) - 3a_3(t - t_d)^2 - 4a_4(t - t_d)^3 - 5a_5(t - t_d)^4 \tag{22}$$

and so on, with a_0 etc. as functions of g and its derivatives at $\tau = t_d$.

Unless the function $f(\tau)$ is specified, a semianalytical integration procedure as was done for the Dirichlet series is not possible. For the general case, one must therefore carry out the integration between $\tau = t_i$ and t_{i+1} by a generalized midpoint rule. The result again can be cast into the formalism of (14), but substitution of (20) into (19) and subsequently into (11) now yields

$$\tilde{E}^{-1}(t^*) = E^{-1}(t^*) + \sum_{\alpha=0}^{N} f(t^*) h_\alpha (t_{i+1} - t_d)(t^*)^\alpha \tag{23}$$

where it is assumed that $E(\tau)$ is piecewise constant, while the viscous term $\tilde{\boldsymbol{\sigma}}$ becomes

$$\tilde{\boldsymbol{\sigma}} = -\tilde{E}(t^*) \sum_{\alpha=0}^{N} [h_\alpha(t_{i+1} - t_d) - h_\alpha(t_i - t_d)]\tilde{\boldsymbol{\varepsilon}}_\alpha(t_i) \tag{24}$$

respectively. The internal variables are updated according to the following recurrence procedure:

$$\tilde{\boldsymbol{\varepsilon}}_\alpha(t_{i+1}) = \tilde{\boldsymbol{\varepsilon}}_\alpha(t_i) + \int_{t_i}^{t_{i+1}} f(\tau)\tau^\alpha \dot{\boldsymbol{\sigma}}(\tau)\, d\tau \approx \tilde{\boldsymbol{\varepsilon}}_\alpha(t_i) + f(t^*)(t^*)^\alpha \Delta\boldsymbol{\sigma} \tag{25}$$

As stipulated before, a semianalytical integration procedure can only be carried out for the Taylor series if the function $f(\tau)$ is known. An important case is the power law

$$J(t, \tau) = E^{-1}(\tau)[1 + q\tau^d(t - \tau)^p] \tag{26}$$

where q, d, and p = material parameters, which formulation is used in the example calculations of stress and damage evolution in a cover element of a breakwater and presented at the end of this article. Now $a_0 = t_d^p$

$$a_{r+1} = a_r \frac{1}{1 + r} \frac{p - r}{t_d}; \qquad r \geq 0 \tag{27}$$

and the series expansion is convergent for $0 < t \leq 2t_d$, since the convergence radius R can be calculated as

$$R = \lim_{r\to\infty} \frac{|a_r|}{|a_{r+1}|} = |t_d| \tag{28}$$

In a fashion similar to that of the derivations in the preceding section, we obtain an incremental stress-strain relation of the form (14), but for the fact that the stiffness can now be obtained by a semianalytical integration procedure

$$\tilde{E}^{-1}(t^*) = E^{-1}(t^*)\left[1 + \sum_{\alpha=0}^{N} \frac{q(t_{i+1}^{\alpha+d+1} - t_i^{\alpha+d+1})}{(\alpha + d + 1)\Delta t} h_\alpha(t_{i+1} - t_d)\right] \tag{29}$$

and that the internal variables $\tilde{\boldsymbol{\varepsilon}}_\alpha$ are not updated via (25), but according to

$$\tilde{\boldsymbol{\varepsilon}}_\alpha(t_{i+1}) = \tilde{\boldsymbol{\varepsilon}}_\alpha(t_i) + \sum_{\alpha=0}^{N} \frac{q(t_{i+1}^{\alpha+d+1} - t_i^{\alpha+d+1})}{E(t^*)(\alpha + d + 1)\Delta t} \Delta\boldsymbol{\sigma} \tag{30}$$

SMEARED-CRACK MODELING

The derivations shown do not take into account the possibility of cracking. However, such an extension can be incorporated straightforwardly if a smeared-crack model is used that is rooted in a decomposition of the strain tensor into a concrete strain $\boldsymbol{\varepsilon}^{co}$ and a crack strain $\boldsymbol{\varepsilon}^{cr}$. Then, the only modification that has to be made is the replacement of the total strain increment $\Delta\boldsymbol{\varepsilon}$ by the concrete strain increment $\Delta\boldsymbol{\varepsilon}^{co}$ in the algorithmic expressions that compute the stress increment $\Delta\boldsymbol{\sigma}$ from the strain increment and the stress or strain history. When we additionally include a thermal strain increment $\Delta\boldsymbol{\varepsilon}^{\theta}$ in the constitutive model, we obtain the following general formalism:

$$\Delta\boldsymbol{\sigma} = \mathbf{D}^{co}(\Delta\boldsymbol{\varepsilon}^{co} - \Delta\boldsymbol{\varepsilon}^{\theta}) + \tilde{\boldsymbol{\sigma}} \tag{31}$$

with

$$\mathbf{D}^{co} = \tilde{E}(t^*)\mathbf{D} \tag{32}$$

where the expressions for $\tilde{E}$ and $\tilde{\boldsymbol{\sigma}}$ read as given in the preceding paragraph for the Dirichlet and Taylor expansions, respectively, so that no modifications are required for the time-dependent concrete model.

Prior to cracking, concrete is modeled as an isotropic, viscoelastic material. When the major principal tensile stress exceeds the tensile strength f_t, that is when a so-called tension cutoff criterion is violated, a crack with a fixed direction is initiated perpendicular to the direction of the major principal stress. Next, a softening branch is entered where the tensile stress normal to the smeared crack is gradually decreased with increasing strain normal to the crack, until a limiting value is reached ε_u where the tensile capacity is exhausted. In modern fracture mechanics concepts (Hillerborg et al. 1976; Bažant and Oh 1983), the area under the stress-strain curve is associated with the fracture energy G_f, which is defined as the energy needed to create a unit area of continuous crack, and is often considered as a material parameter. For young concrete, the fracture energy is a function of time (Brameshuber and Hilsdorf 1989), so that introduction of the quantity as a fixed material parameter does not seem sensible for the present purpose. In consideration of the limited amount of experimental evidence in the literature on the fracture mechanics properties of young concrete, a simple

approach is adopted in the example calculations, whereby ε_u is specified as model parameter instead of the fracture energy G_f.

The additive decomposition of the total strain into a concrete part $\boldsymbol{\varepsilon}^{co}$ and a cracking part $\boldsymbol{\varepsilon}^{cr}$ reads in an incremental form (de Borst and Nauta 1985; de Borst 1987; Rots 1988)

$$\Delta\boldsymbol{\varepsilon} = \Delta\boldsymbol{\varepsilon}^{co} + \Delta\boldsymbol{\varepsilon}^{cr} \tag{33}$$

As pointed out by de Borst and Nauta and de Borst (1987) the crack strain increment $\Delta\boldsymbol{\varepsilon}^{cr}$ can again be composed of several contributions

$$\Delta\boldsymbol{\varepsilon}^{cr} = \Delta\boldsymbol{\varepsilon}_1^{cr} + \Delta\boldsymbol{\varepsilon}_2^{cr} + \cdots \tag{34}$$

where $\Delta\boldsymbol{\varepsilon}_1^{cr}$ = strain increment owing to a primary crack; $\Delta\boldsymbol{\varepsilon}_2^{cr}$ = strain increment owing to a secondary crack, and so on. For simplicity's sake, this enhancement is not pursued here.

The relation between the crack strain increment of a particular crack (either primary or secondary) and the stress increment is conveniently defined in the coordinate system that is aligned with the crack. This necessitates a transformation between the crack strain increment $\Delta\boldsymbol{\varepsilon}^{cr}$ of crack n in the global x, y–coordinate system and a crack strain increment $\Delta\mathbf{e}^{cr}$ that is expressed in local n, t–coordinates. Restricting the treatment to a two-dimensional configuration (which is not essential), we observe that a crack only has a normal strain increment Δe^{cr} (mode I) and a shear strain increment $\Delta\gamma^{cr}$ (mode II), so that

$$\Delta\mathbf{e}^{cr} = (\Delta e^{cr}, \Delta\gamma^{cr})^T \tag{35}$$

The relation between $\Delta\boldsymbol{\varepsilon}^{cr}$ and $\Delta\mathbf{e}^{cr}$ reads

$$\Delta\boldsymbol{\varepsilon}^{cr} = \mathbf{N}\Delta\mathbf{e}^{cr} \tag{36}$$

with

$$\mathbf{N} = \begin{bmatrix} \cos^2\phi & -\sin\phi\cos\phi \\ \sin^2\phi & \sin\phi\cos\phi \\ 2\sin\phi\cos\phi & \cos^2\phi - \sin^2\phi \end{bmatrix} \tag{37}$$

and ϕ = inclination angle of the normal of the crack with the x-axis. In a similar way, we can define a vector $\Delta\mathbf{s}$

$$\Delta\mathbf{s} = (\Delta s, \Delta t)^T \tag{38}$$

with Δs being the normal and Δt the shear stress increment in the crack coordinate system. The relation between the stress increment in the global coordinate system $\Delta\boldsymbol{\sigma}$ and the stress increment vector $\Delta\mathbf{s}$ reads

$$\Delta\mathbf{s} = \mathbf{N}^T\Delta\boldsymbol{\sigma} \tag{39}$$

To complete the system of equations, we use the general form of the integrated evolution equations for viscoelasticity (31) as constitutive relation for the concrete and a stress-strain relation for the smeared cracks that we assume to have the following format:

$$\Delta\mathbf{s} = \mathbf{D}^{cr}\Delta\mathbf{e}^{cr} + \boldsymbol{\Lambda} \tag{40}$$

where $\mathbf{D}^{cr}$ = a 2 × 2 matrix; and $\boldsymbol{\Lambda}$ = a vector that contains the viscous or rate effects in the cracks. Using (31)–(40), we can develop the tangential stiffness relation for the cracked concrete

$$\Delta\boldsymbol{\sigma} = [\mathbf{I} - \mathbf{D}^{co}\mathbf{N}(\mathbf{D}^{cr} + \mathbf{N}^T\mathbf{D}^{co}\mathbf{N})^{-1}\mathbf{N}^T][\mathbf{D}^{co}(\Delta\boldsymbol{\varepsilon} - \Delta\boldsymbol{\varepsilon}^0) + \tilde{\boldsymbol{\sigma}}] + \mathbf{D}^{co}\mathbf{N}(\mathbf{D}^{cr} + \mathbf{N}^T\mathbf{D}^{co}\mathbf{N})^{-1}\boldsymbol{\Lambda} \quad (41)$$

The addition of a viscous component to the crack stress prevents the rate-boundary value problem from becoming ill-posed. This holds true for truly dynamic analyses (Sluys 1992) as well as for slow processes as considered here (de Borst et al. 1993). On the other hand, inclusion of viscous terms in the stress-strain relation for the concrete [$\tilde{\boldsymbol{\sigma}}$ in (31)] does not preserve well-posedness of the rate-boundary value problem.

COMPARISON WITH EXPERIMENTAL RESULTS

The application of the power-law model to the prediction of the creep and relaxation behavior of hardening cement paste needs realistic values of the parameters q, d, and p. A direct use of values that are found in the literature (e.g., Bažant and Osman 1976; van Breugel 1991) is difficult, since similar parameters are often used in a slightly different form. Moreover, the specific values depend on the hardening conditions (humidity, temperature, etc.) and the amount and type of cement. The shrinkage caused by drying of the hardening cement paste is taken into account in an implicit fashion, namely by incorporating its effect in the values of q, d, and p.

Van Heyningen and Boon (1973) measured the development of the temperature, the Young's modulus, and the stresses in concrete cubes in a stiff frame. The numerical simulation is performed using one element with a linear coefficient of thermal expansion of $0.011 \cdot 10^{-3}$ K^{-1}. Figs. 2 and 3 show the evolution of the Young's modulus and the stress, respectively, in the first 7 days for different combinations of the parameters. We observe a reasonable agreement between the model simulation and the experimental results, although the prediction of the time at which the stress has its largest

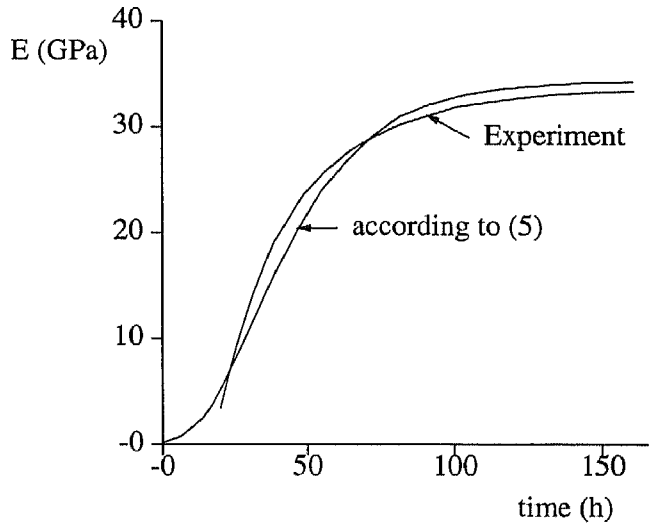

FIG. 2. Evolution of Young's Modulus in Concrete Cube in Stiff Frame—Comparison between Experiment (Van Heyningen and Boon 1973) and Simulation According to Eq. (5)

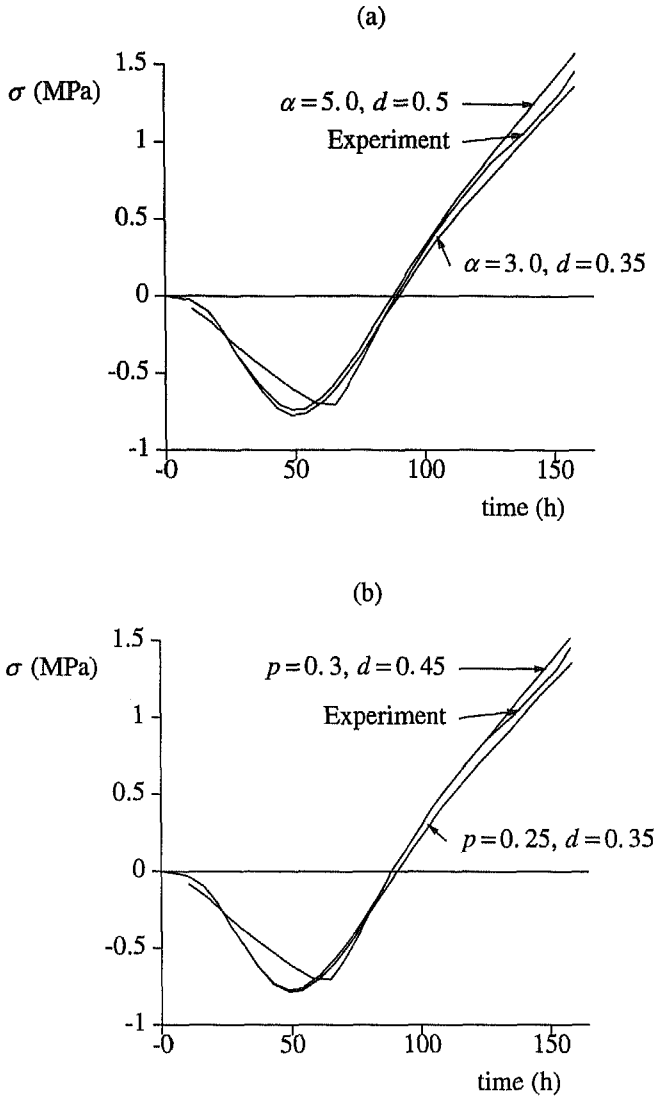

FIG. 3. Stress Evolution in Concrete Cube in Stiff Frame—Comparison between Experiment (Van Heyningen and Boon 1973) and Simulation According to Eq. (5): (a) $p = 0.3$ with Different Values for q and d; and (b) $q = 4.0$ with Different Values for p and d

compressive value is too early. When the prediction of crack formation is the primary goal of the analysis, the inaccuracies in the first 2 days are less important, since cracking takes place during the cooling process. It is finally noted that the range of parameter values used here reasonably compares with values quoted by other investigators (Bažant and Osman 1976; van Breugel 1991), especially those for d and p.

EXAMPLE CALCULATIONS

An example is now presented that was computed with the DIANA finite-element program. It involves the calculation of the stresses during the hardening process in early-age concrete. The structure considered is a tetrapod, which is used as a cover element for a breakwater. The full structure has

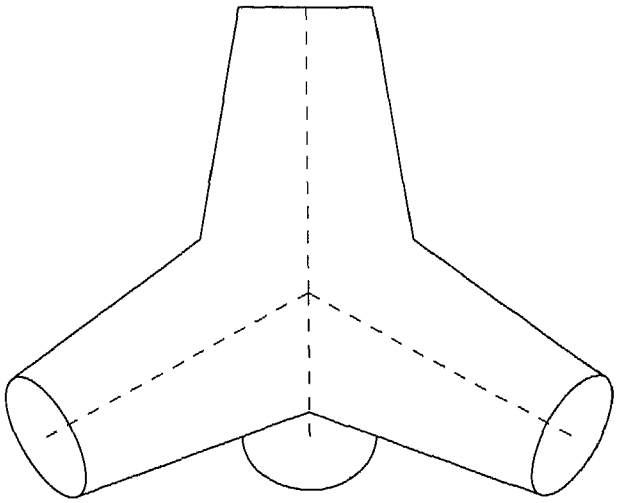

FIG. 4. Three-Dimensional Picture of Tetrapod Structure

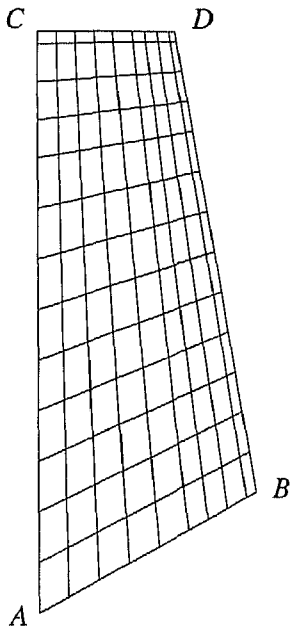

FIG. 5. Discretization of One Leg of Tetrapod Structure

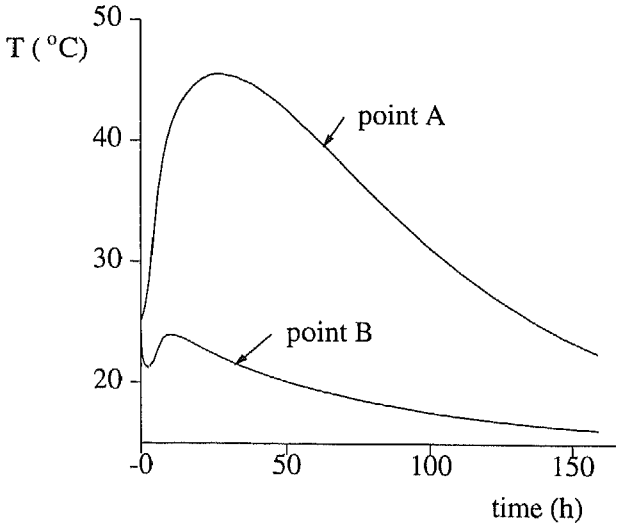

FIG. 6. Evolution of Temperature in Points A and B of Tetrapod

four axisymmetric legs as shown in Fig. 4. In the analyses described here, one leg was modeled, and it was assumed that full axisymmetry could be adopted, including the boundary AB. This is a simplification, since the connection with the other legs of the tetrapod can never be axisymmetric. The element mesh for the stress calculation of one leg is shown in Fig. 5. In line with the assumption of full axisymmetry, smooth boundary conditions were imposed along AB and AC. In the thermal analysis, an initial temperature of 25°C in the interior of the tetrapod was given. The temperature of the environment was 15°C, and special interface elements were used at these boundaries to model the convection (convection coefficient 0.025 kW/m^{2}K). No heat flow was permitted along the axis of axisymmetry AC and edge AB. The model defined by (1)–(4) was used with $\lambda_0 = 4 \cdot 10^{-3}$ kW/mK, $\lambda_1 = 1.4 \cdot 10^{-3}$ kW/mK, $c_0 = 2{,}950$ kJ/m^{3}K, $c_1 = 300$ kJ/m^{3}K, $Q_\infty = 73{,}528$ kJ, $\gamma = 0.72 \cdot 10^9$ kJ/s, and $b = 6{,}000$ K. The evolution of Young's modulus was calculated according to (5) with the parameters $E_0 = 20{,}000$ MPa and $\beta = 0.075$. Because of the heat generation in the hydration process, the temperature in the interior of the leg rises. For a leg diameter of 2 m it reaches a value of approximately 46°C. Fig. 6 shows that the difference between the temperatures in the interior of the tetrapod and the exterior may amount up to 25°C.

In the stress analysis, the power law of (26) was used with the parameters $q = 4.518$, $d = 0.35$, $p = 0.3$, and a development time $t_d = 0.3024 \cdot 10^6$ s. The linear coefficient of thermal expansion was $0.011 \cdot 10^{-3}$ m/mK. Poisson's ratio was taken equal to 0.2. Rate effects were not considered for the smeared-crack model ($\Lambda = 0$). In the reference calculation, the tensile strength was taken equal to $f_t = 2$ MPa, and a linear softening branch was adopted with an ultimate strain $\varepsilon_u = 0.033$, at which the tensile capacity is exhausted.

For the stress analysis, eight-noded isoparametric elements were used with a 3 × 3 Gaussian integration. The finite-element calculations were carried out in 31 time steps, starting with increments of 1 h up to increments

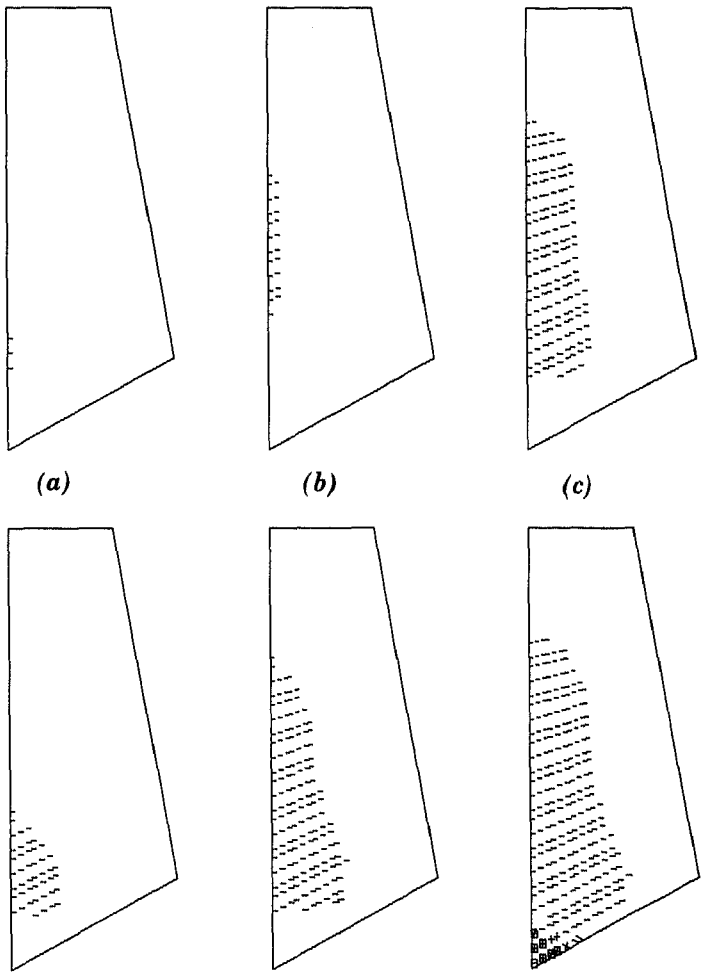

FIG. 7. Crack Patterns for t = 100 h (Top) and t = 150 h (Bottom): (*a*) D = 1.5 m; f_t = 2.0 MPa; (*b*) D = 2.0 m; f_t = 2.0 MPa; and (*c*) D = 2.0 m; f_t = 1.5 MPa

of 10 h for the last 10 steps. A modified Newton-Raphson procedure was used to achieve equilibrium within each time step. The convergence criterion was based on the Euclidean norm of the incremental displacements and was set equal to 10^{-3}. Normally, 8–12 iterations were needed to comply with this requirement, but at extensive cracking this number increased to 19.

The crack patterns that result from the finite-element simulations are shown in Fig. 7 for t = 100 h and t = 150 h. Each dash corresponds to a cracked integration point and the direction of the dash coincides with the crack surface direction (orthogonal to the major principal tensile stress), but the size of the dashes has no physical meaning. The little rectangles in the pictures at t = 150 h represent cracking due to tensile hoop stresses. Fig. 7(*b*) represents the standard case with a tensile strength f_t = 2 MPa and a diameter of the leg of the tetrapod D = 2 m. Fig. 7(c) is for the same

structural size, but for a lower tensile strength (f_t = 1.5 MPa), and Fig. 7(*a*) shows the crack evolution for the same tensile strength, but for a smaller diameter (D = 1.5 m). We observe the faster spreading of the cracking for the larger diameter and for the smaller tensile strength. Also, the zones in which cracks propagate are different.

CONCLUDING REMARKS

An algorithm was derived that allows finite-element computations of stress evolution and (smeared) crack propagation in young, maturing concrete. Realistic simulations can be obtained with the model, although the predictive value of the computations can be further enhanced by improved constitutive models for the stiffness evolution, the creep behavior, and the fracture properties of early-age concrete.

APPENDIX I. REFERENCES

Anderson, C. A., Bažant, Z. P., Buyukozturk, O., Jonasson, J.-E., and Willam, K. (1988). "Finite element analysis of creep and shrinkage." *Mathematical modeling of creep and shrinkage of concrete*, Z. P. Bažant, ed., J. Wiley & Sons, Chichester, England, 275–310.

Bažant, Z. P., Dougill, J., Huet, C., Tsubaki, T., and Wittmann, F. H. (1988). "Material models for structural creep analysis." *Mathematical modeling of creep and shrinkage of concrete*, Z. P. Bažant, ed., J. Wiley & Sons, Chichester, England, 275–310.

Bažant, Z. P., and Oh, B. (1983). "Crack band theory for fracture of concrete." *Mat. and Struct.*, RILEM, 16, 155–177.

Bažant, Z. P., and Osman, E. (1976). "Double power law for basic creep of concrete." *Mat. and Struct.*, RILEM, 9, 3–11.

Bažant, Z. P., and Wu, S. T. (1973). "Dirichlet series creep function for aging concrete." *J. Engrg. Mech. Div.*, ASCE, 99, 367–387.

Bažant, Z. P., and Wu, S. T. (1974). "Rate-type creep law of aging concrete based on Maxwell chain." *Mat. and Struct.*, RILEM, 7, 45–60.

Brameshuber, W., and Hilsdorf, H. K. (1989). "Development of strength and deformability of very young concrete." *Fracture of concrete and rock*, S. P. Shah and S. E. Swartz, eds., Springer-Verlag, New York-Berlin-Heidelberg, 409–421.

de Borst, R. (1987). "Smeared cracking, plasticity, creep and thermal loading—a unified approach." *Comp. Meth. Appl. Mech. Engrg.*, 62, 89–110.

de Borst, R. (1989). "Thermal stresses." *Fracture mechanics of concrete structures: from theory to applications*, L. Elfgren, ed., Chapman and Hall, London and New York, 148–154.

de Borst, R., and Nauta, P. (1985). "Non-orthogonal cracks in a smeared finite element model." *Engrg. Comput.*, 2, 35–46.

de Borst, R., van den Boogaard, A. H., van den Bogert, P. A. J., and Sluys, L. J. (1993). "Computational issues in time-dependent deformation and fracture of concrete." *Proc., Fifth RILEM Int. Symp. on Creep and Shrinkage of Concrete*, Z. P. Bažant and I. Carol, eds., E. & F.N. Spon, London and New York, 390–407.

Hillerborg, A., Modeer, M., and Petersson, P. E. (1976). "Analysis of crack formation and crack growth in concrete by means of fracture mechanics and finite elements." *Cement and Concrete Res.*, 6, 773–782.

Reinhardt, H. W., Blaauwendraad, J., and Jongedijk, J. (1982). "Temperature development in concrete structures taking account of state dependent properties." *Proc., Int. Conf. Concrete at Early Ages*, Paris, France.

Rots, J. G. (1988). "Computational modelling of concrete fracture," PhD dissertation, Delft University of Technology, Delft, The Netherlands.

Sluys, L. J. (1992). "Wave propagation, localisation and dispersion in softening solids," PhD dissertation, Delft University of Technology, Delft, The Netherlands.

Taylor, R. L., Pister, K. S., and Goudreau, G. L. (1970). "Thermomechanical analysis of viscoelastic solids." *Int. J. Num. Meth. Engrg.*, 2, 45–60.
van Breugel, K. (1991). "Simulation of hydration and formation of structure in hardening cement-based materials," PhD dissertation, Delft University of Technology, Delft, The Netherlands.
van den Bogert, P. A. J., de Borst, R., and Nauta, P. (1987). "Simulation of the mechanical behavior of young concrete." *IABSE Rep.*, 54, 339–347.
van Heyningen, B., and Boon, J. (1973). "Onderzoek naar het gedrag van jong beton ten behoeve van de tunnel te Vlake (an investigation into the behavior of young concrete for the Vlake tunnel)." *Rep. B-73-214*, TNO-IBBC, Delft, The Netherlands (in Dutch).
Zienkiewicz, O. C., Watson, M., and King, I. P. (1968). "A numerical method of viscoelastic creep analysis." *Int. J. Mech. Sci.*, 10, 807–827.

APPENDIX II. NOTATION

The following symbols are used in this paper:

a_α = coefficients;
b = material parameter;
$\mathbf{C}$ = matrix;
c = heat capacity;
c_0 = material parameter;
c_1 = material parameter;
$\mathbf{D}$ = matrix;
$\mathbf{D}^{co}$ = concrete stiffness matrix;
d = material parameter;
E = Young's modulus;
E_0 = elastic stiffness parameter;
E_α = elastic stiffness of chain element;
$\bar{E}$ = instantaneous stiffness;
e^{cr} = normal crack strain;
$\mathbf{e}^{cr}$ = crack strain tensor in local coordinates;
f = heat-production function;
f = age-dependent function;
f_t = tensile strength;
G_f = fracture energy;
g = function,
h_α = polynomial;
J = creep function;
$\mathbf{N}$ = transformation matrix;
n = local coordinate;
p = material parameter;
r = degree of maturity;
q = heat production;
q = material parameter;
Q_∞ = total heat production per unit volume;
s = normal stress in local coordinate system;
$\mathbf{s}$ = stress tensor in local coordinate system;
T = absolute temperature;
T_0 = 273 K;
t = local coordinate;
t = shear stress in local coordinate system;

t = time;
t_d = development time;
x = global coordinate;
y = global coordinate;
α = counter;
β = delay factor;
γ = material parameter;
γ^{cr} = shear crack strain;
Δ = increment;
δ_{ij} = Kronecker delta;
ε_u = ultimate strain;
$\boldsymbol{\varepsilon}$ = strain tensor;
$\boldsymbol{\varepsilon}^{co}$ = concrete strain tensor;
$\boldsymbol{\varepsilon}^{cr}$ = crack strain tensor;
$\boldsymbol{\varepsilon}^{\theta}$ = thermal strain tensor;
$\tilde{\boldsymbol{\varepsilon}}_\alpha$ = tensor containing internal variables;
$\boldsymbol{\Lambda}$ = vector for rate effects;
λ = thermal conductivity;
λ_0 = material parameter;
λ_1 = material parameter;
λ_α = retardation time;
$\boldsymbol{\nu}$ = Poisson's ratio;
$\boldsymbol{\sigma}$ = stress tensor;
$\tilde{\boldsymbol{\sigma}}$ = relaxation tensor; and
ϕ = inclination angle of crack.